Electrohydrodynamic air amplifier for low-energy airflow generation – experimental proof-of-concept

Donato Rubinetti [1,2 *], Kamran Iranshahi [1,3], Daniel Onwude[1], Bart M. Nicolaï [2], Lei Xie [4], Thijs Defraeye [1,5]

[1] Empa, Swiss Federal Laboratories for Materials Science and Technology, Laboratory for Biomimetic Membranes and Textiles, Lerchenfeldstrasse 5, CH-9014 St. Gallen, Switzerland

[2] KU Leuven, Katholieke Universiteit Leuven, Faculty of Bioscience Engineering, Kasteelpark Arenberg 20, BE-3001 Leuven, Belgium

[3] ETH-Zurich, Swiss Federal Institute of Technology, Zurich 8092, Switzerland

[4] Belimed AG, Grienbachstrasse 11, CH-6300 Zug, Switzerland

[5]Dalhousie University, Faculty of Agriculture, Truro, Nova Scotia, Canada

Electrohydrodynamic (EHD) air amplification is a novel way to generate airflow with low energy consumption. This study experimentally evaluates how air amplification via the Coanda effect raises the overall flow rate performance of EHD airflow generation. Due to the complex multiphysical nature of EHD air amplification, the design stages are investigated one by one starting with a simple emitter-collector configuration. First, regular EHD flow was studied in a 150×150×500 mm^3 channel. Then, a dielectric material was added to determine its influence on the electric field. The impact of a converging nozzle on the EHD-generated airflow was subsequently studied. Lastly, the converged nozzle airflow was used as a supply air stream on a plate to facilitate air amplification of the surrounding air. We show the proof of concept for an EHD air amplification system. After a voltage threshold of 14 kV, amplified airstreams up to an amplification factor of 3 were measured. Maximum airflow rates of about 15 $m^3\ h^{-1}$ were obtained shortly before electric breakdown at 22 kV. Compared to regular EHD, we achieved a higher flow rate for the same electric energy invested. As a measure of efficiency, the flow rate per electric power increased up to 66 % in EHD air amplification with normal EHD as the benchmark. The proposed EHD air amplifier operates at atmospheric pressures and lays the groundwork for further optimization studies to position EHD air amplification as an alternative to conventional fans or standard EHD airflow generation.

Keywords: Air amplification, Alternative air propulsion, Corona discharge, Low power ventilation

[*] *Corresponding author: thijs.defraeye@empa.ch (T. Defraeye) Empa, Swiss Federal Laboratories for Materials Science and Technology, Laboratory for Biomimetic Membranes and Textiles, Lerchenfeldstrasse 5, CH-9014 St. Gallen, Switzerland*

1 Introduction

Airflow generation is ever-present with applications ranging from large-scale jet propulsion engines to domestic hand-held hairdryers. The need to move air is predominantly satisfied by rotating impellers or other mechanical devices with blades. Electrohydrodynamic (EHD) air propulsion, on the other hand, is a way to produce flow rates without moving parts. In EHD airflow generation, an airflow is induced due to a high voltage gradient between a sharply curved electrode (i.e. emitter) and a collecting ground electrode (i.e. collector). An area of ionized air develops around the emitter, which travels from emitter to collector. In transition, the ionized air molecules collide with neutral air molecules, thus, inducing an airflow, also known as ionic wind [1]. Although the air ionization process is energy-efficient [2], reaching high EHD flow rates can be challenging from the high voltage engineering point of view.

Several EHD improvement attempts have been made to position EHD as a viable alternative to conventional rotary air movers. Efforts were made on (1) the modification of the electric field with secondary non-ionizing electrodes [3], [4], (2) optimization of electrode shapes [5], (3) grouping units of ionic wind devices into an array [6] and (4) multi-stage EHD pump designs [7]. Ultimately, these studies and many others attempt to increase the velocity component of the airspeed parallel to the desired flow direction. To a certain extent these efforts are successful, but also highly dependent on the given setup or electrode arrangement, respectively. This is due to the ions following the electrical field lines as they propagate from emitter to collector electrode. In turn, the cloud of ions distort the electric field which can cause inefficiencies in momentum transfer, especially at elevated voltages of about 30 kV. Moreover, any non-dielectric material in proximity of the electrodes also perturbates the electric field. Optimizing EHD flow rates on the electrostatic side is, therefore, a challenge better tackled with numerical tools due to the vast design space. This study focuses on improving the flow rate aerodynamically by exploiting the Coanda effect as air amplifying mechanism.

The Coanda effect is the tendency of a primary fluid stream to remain attached to a nearby solid wall [8], [9]. The surrounding air is then dragged along under pressure, thus, inducing a secondary fluid stream. This enables the primary stream (supply) to create a much larger bulk flow due to the amplification of the former. Industrial solid-state air amplifiers typically use pressurized air sources, which require energy-intensive air supply equipment. Even commercially available air amplifiers are not a worthy replacement for conventional fans for bladeless ventilation. That is the inherent problem of both EHD and air amplifiers: they are energy inefficient as stand-alone technologies and, therefore, uninteresting as a replacement for conventional fans. EHD is inefficient due to its low electrical to mechanical energy conversion rate [10], and air amplifiers are inefficient due to a large amount of energy necessary to compress its air supply. However, by linking EHD to air amplification we can reduce inefficiencies.

Prior to this study, a numerical EHD air amplification proof-of-concept study has been conducted [11]. There, we found that combining EHD with the Coanda effect can improve the flow rate to electrical power ratio up to 59 %. In this study, we aim to investigate the advantages of combining the low-energy, low-pressure EHD flow technology with air amplification technology experimentally using a customizable rig. This is necessary to separate electrostatic phenomena and airflow phenomena such that a straightforward EHD air amplifier design can be built. First, we study free flow EHD in a 150×150×500 mm^3 channel with needles and wire as ionizing electrodes. We then proceed with the introduction of dielectrics and nozzles to check the stability of the discharge. Finally, the findings lead to a design capable of EHD air amplification. We also assess relevant performance metrics such as electric power consumption, flow rate, flow rate per power invested and amplification factor. These metrics are compared to regular EHD designs with needles and wires as emitting electrodes. Furthermore, the results are compared to commercially available regular air amplifiers and a conventional fan.

2 Technology overview on air amplification

Air amplification is an established technology to enhance airflow without moving parts. A variety of shapes and configurations exists, i.e., circular air amplifiers or air knives. These solid-state devices convert an airstream of pressurized air into a more significant bulk flow by exploiting aerodynamic phenomena, e.g., air induction via the Coanda effect and air entrainment. Such phenomena arise when a primary airstream (e.g., from pressurized air) slides along a surface. Then, a secondary airstream is induced and increases the overall flow rate. The ratio between secondary (induced and entrained) and primary (supply) airflow rate is the amplification factor. In contrast to regular fan-based flow generation, air amplifiers have no mechanical moving parts, making them an exciting technology in areas where low maintenance, silent equipment is pivotal.

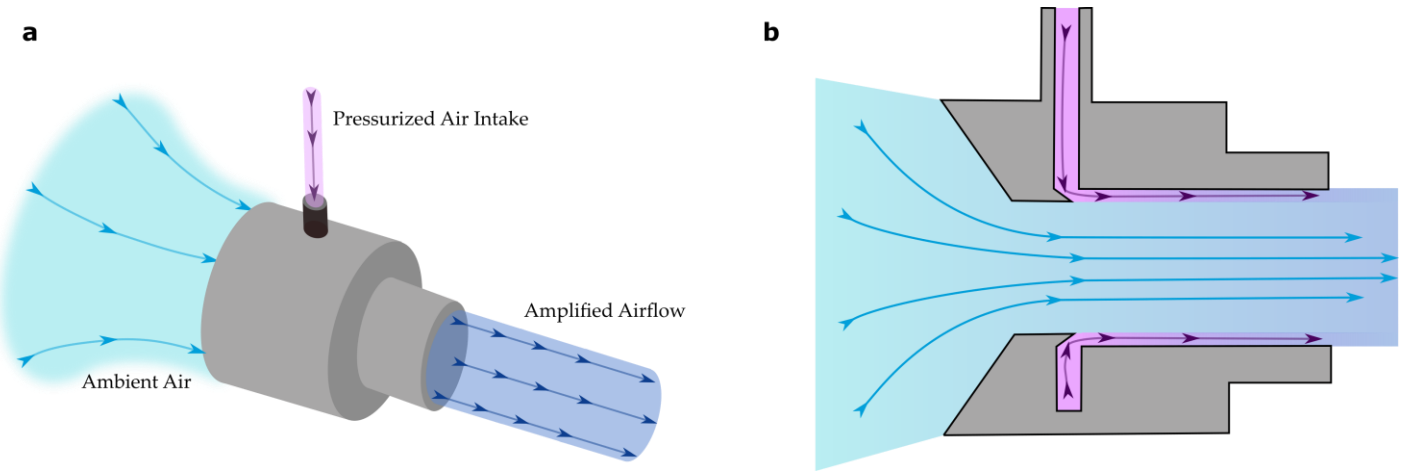

Figure 1: Example of an air amplifier fed by presszurized air with (a) showing the working principle and (b) the cross-section including flow paths.

Commercially available industrial air amplifiers, such as the Meech (Meech International, 2 Network Point, Range Road, Witney, OX29 0YN, UK) Air Amplifier (A15xxx series) and High Thrust Jet (A38xxx series), need a supply pressure of 1.4 to 7 bar for successful operation. An amplification factor of 4 to 25 is achieved depending on the device's inner diameter (18 – 100 mm for the Air Amplifier and 9 – 34 mm for the High Thrust Jet). For domestic applications, Dyson (DYSON HOME TECHNOLOGIES PTE. LTD., 2 Science Park Drive, Singapore) offers several products with air amplification technology. These products range from hand-held hair dryers (Dyson Supersonic™, 46.8 m^3/h, 1600 W) to domestic ventilators (Dyson Purifier Cool™, 1044 m^3/h, 40 W). In contrast to pressurized air-based amplifiers, the Dyson products are powered by an enclosed impeller.

3 Materials and methods

3.1 Lab setups for EHD air amplification

We constructed several experimental setups. The base setup with peripheral components and measurement devices is described in section 3.1.1. In section 3.1.2, different test rigs are evaluated, which split up the different physical phenomena that have an effect on in EHD air amplification. We start from an EHD airflow generation device with an emitter electrode and an large mesh collector. The first step is evaluating the size impact of the collector. Second, we evaluate the impact of the presence of a dielectric, since the housing of the air amplifier can affect the EHD generated airflow. Third, we quantify how the airflow contraction, which is present in the air amplifier, affects the EHD generated flow. Finally, we combine the reduced mesh collector, the dielectric, and the airflow contraction with an external wall, on which the Coanda effect establishes. With this setup, we can quantify the air entrainment of the surrounding air induced by the EHD airflow generation. The idea behind this stepwise approach is that we can analyze and troubleshoot every phenomena and associated part in the new device.

3.1.1 EHD airflow base setup

Figure 2 shows the base setup of our rig that is customizable to accommodate changes in geometry. The main components are a 150 x 150 x 500 mm^3 square cross-section channel made of 5 mm acrylic glass plates. Inside there are the electrical components such as the emitter and collector. The four emitter electrodes have a tip radius of 40 microns and are equally spaced from each other. The collector consists of soldered 1 mm diameter steel wires with 10 mm spacing in between them. This mesh collector lets the accelerated airflow pass through while still acting like a straight wall for the ions. The electrodes are connected to a high voltage DC power supply (Spellmann SL30PN10) of positive polarity. The hot-wire anemometer (Testo 405i) is placed downstream at the end of the channel to measure a point-wise velocity. For safety reasons, the rig is placed within a customized (1 x 1 x 2 m^3) Faraday cage-like environment to meet high voltage precautions.

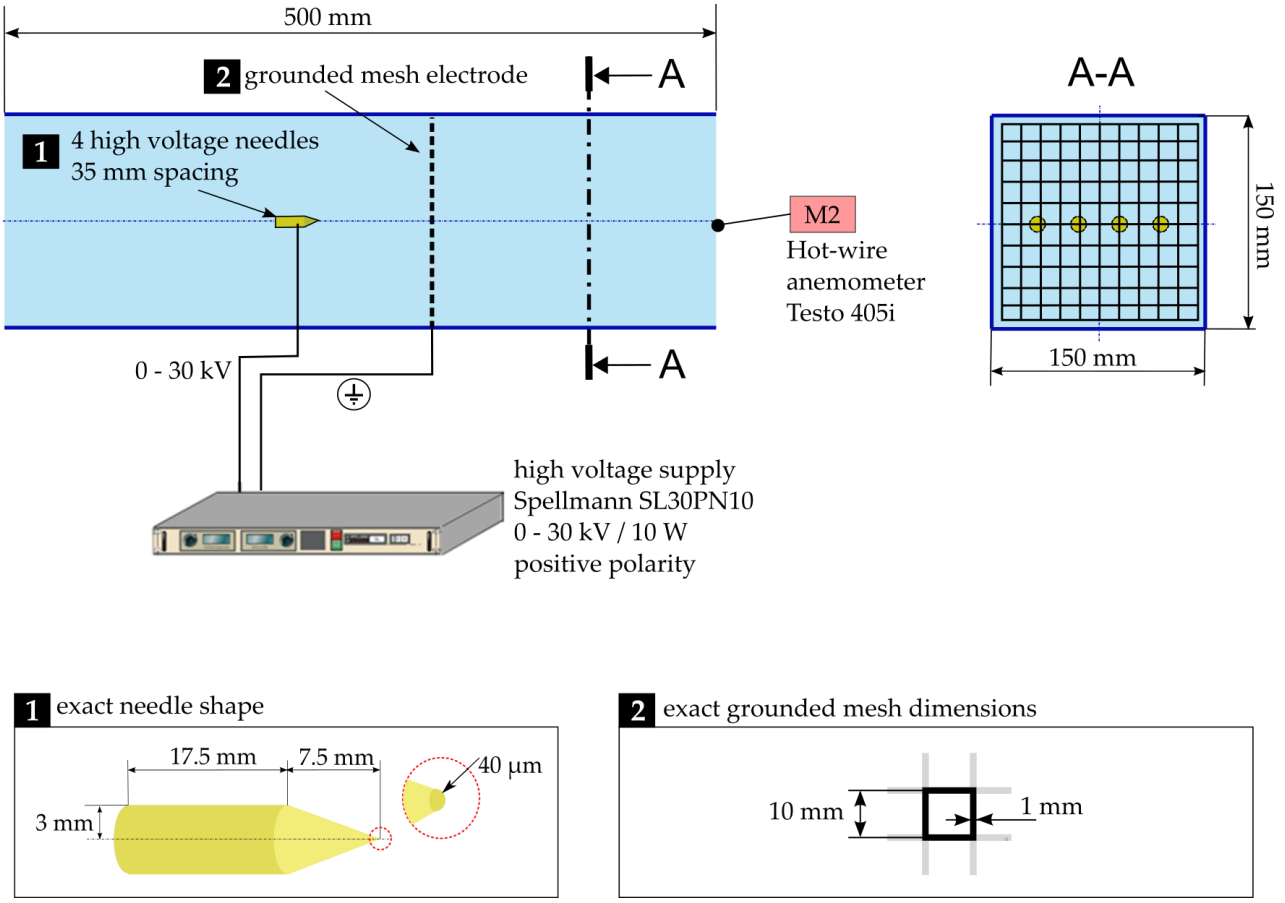

Figure 2: Base setup of the test rig with peripheral components. The electrical components (4 emitter needles and a large mesh collector) are accommodated in a 150 x 150 x 500 mm³ channel made of transparent acrylic plates. This base configuration produces EHD airflow without amplification and serves as starting point for the step-wise exploration of EHD air amplification. M2 is the point probe measurement location at the outlet for airspeed.

3.1.2 Experimental setup to identify the different phenomena in EHD air amplification

To establish a self-sustaining and continuous Corona discharge that would yield a measurable airstream in a compact area we investigate the influence of several interconnected factors in EHD air amplification. This was done in a step-wise manner to approach EHD air amplification conditions straightforwardly as in Figure 3.

(a) *EHD base configuration.* This configuration is the basis EHD operates in free-flow mode. The arrangement as seen in Figure 3a is the most basic EHD air propulsion technique intended to define the range of operation voltage-wise.

(b) Reduced mesh size and distance to test downsizing possibilities. Here, the large mesh collector is replaced by a same-type mesh strip of 10 x 150 mm² size, see Figure 3b. The first experimental runs are carried out at an inter-electrode distance of $\delta = 50$ mm analogously to the base case (A). The subsequent runs are done with a reduced distance of $\delta = 25$ mm. This step introduces the necessary downsizing for the mesh collector to study the effect of the dimensions and arrangement of the grounded mesh collector.

(c) Introduction of dielectric to assess the stability of the discharge. This step according to Figure 3c is intended to study the influence of an approaching dielectric on the operation range. Introducing a dielectric has implications on the distribution of electric field lines which may cause instabilities in the self-sustaining discharge. Based on the configuration (B), this step introduces two additional horizontal acrylic glass plates of 5 mm thickness with variable distance in between. The distance is $h = 15, 35$ or 85 mm. In the intended initial setup, the wire was in an enclosure of 10 mm, which seemed to create a more homogeneous electric field in the proximity of the emitter, which impedes a continuous discharge. Here, the influence of a nearby dielectric on the necessary inhomogeneity of the electric field is checked by narrowing the gap.

(d) Introduction of the converging nozzle to concentrate the airflow. In this step, the aerodynamic performance of EHD is checked when a converging nozzle is present as per Figure 3d. Flow concentration is essential to create a bleed stream of airflow which can, in turn, be used to amplify airflow rates of a secondary channel. The nozzle gap is $\varepsilon = 10$ and 20 mm.

(e) *Channel extension and introduction of Coanda effect for EHD air amplification*. Ultimately, steps (a)-(d) give a guideline on designing an EHD air amplifier, which results in an extended channel as in Figure 3e. The extension features a flat plate attached to the nozzle where the EHD-generated airjet can flow along. The bottom part of the extended channel is closed such that a clear separation of air domains is established. EHD air amplification is successful when an airspeed is measured at location M3. This means that ambient air is accelerated by flow induction arising from the Coanda effect. The Coanda effect happens when the flow escaping the nozzle remains attached to the solid wall due to pressure asymmetries and thus leads to a greater overall bulk flow. Location M1 measures the EHD-related inflow only and M2 measures the total outflow. In general, and also in points (a) to (d), M1 and M2 record the airflow at the in- and outlet, respectively. We assume partially developed channel flow. A more representative measurement could be the determination of the velocity profile at both M2 and M3. For the proof-of-concept, point measurements are sufficient.

With this step-wise approach, it is possible to clearly distinguish the influence of the various parameters on the complex multiphysical nature of EHD air amplification. Setups (a) to (c) focus on the electrostatic part of the problem while (d) deals with the fluid dynamics. For comparison purposes, all the runs are also repeated with a wire instead of needles. The performance analysis revealed that wire emitter is unpractical for an EHD air amplifier, so only the needles are considered as emitter for (e), i.e., the final EHD air amplifier proof-of-concept.

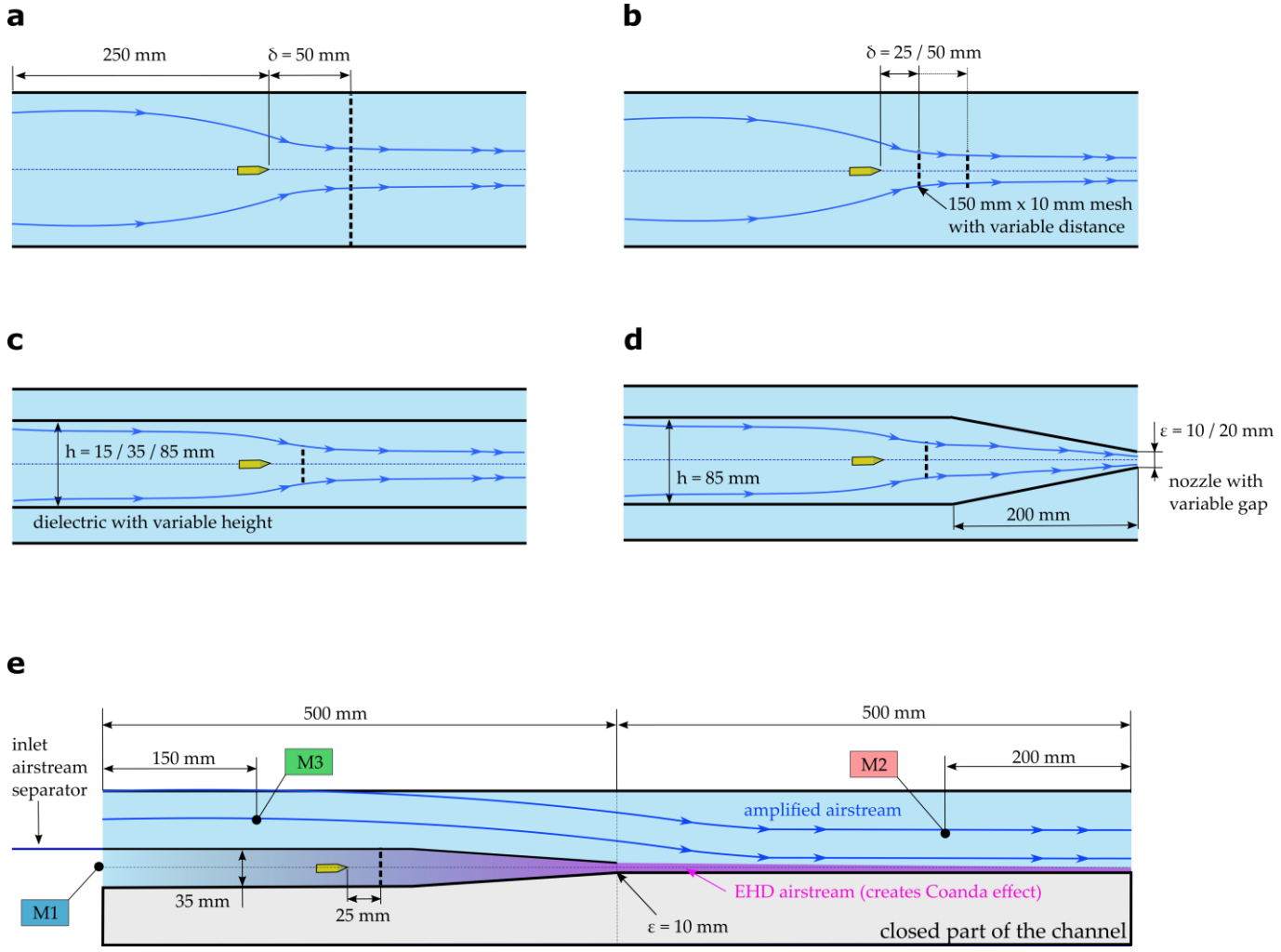

Figure 3: Five configurations step-wise approaching EHD air amplification. (a) is the base configuration, (b) introduces a reduced mesh and closer inter-electrode gap. (c) features two acrylic-glass plates with variable distance to study the influece of a nearby dielectric. (d) includes a converging nozzle to examine the effect of flow contraction. (e) is the final version of the EHD air amplifier where the channel extension allows for the creation of the Coanda effect.

The final EHD air amplifier is based on the previous results obtained in (a) to (d). It consists of an extended channel where the emitter and collector are embedded in the first half of the channel, 500 mm in length. The needles are placed in a 35 mm space, which ends in a converging nozzle, thus creating a primary stream of higher velocity as air is pushed through the gap. Adjacent to the gap is the extension of the channel with another acrylic glass plate to carry the EHD airstream. The entire configuration can be separated into three air volumes, (i) the free stream domain, i.e., the intended amplified airstream region in the upper half of the channel; (ii) the EHD airflow space and (iii) the closed part of the channel. In the closed part, airflow is inhibited to establish air amplification via a Coanda effect on the upper half. At the channel's beginning, an inlet airstream separator is additionally mounted to clearly distinguish between EHD-induced inflow and amplified inflow.

3.2 Measurements and experimental procedure

Measurements were carried out for airspeed (M1-M3), electric current, air temperature, and humidity. The airflow point probes are located as shown in Figure 2 and Figure 3e, while voltage and current are directly read from the high voltage power supply. Previous to the experiments, the validity of displayed current and voltage were verified with multimeter measurements to verify the validity of the current displayed on the power supply. Note that voltage is also the regulating variable while the current setting is maxed out. Temperature and humidity measurements are done via a Sensirion SHT31 sensor (SENSIRION AG, Laubisruetistrasse 50, 8712 Staefa, Switzerland. Accuracy on humidity +/- 1.5 % and +/- 0.1 °C on temperature).

The voltage increases from 0 kV until breakdown voltage (i.e., the voltage when the electric field strength is too high to sustain a Corona discharge and produces arc discharge instead) to determine the operating range. The operation starting point was determined only when both an electric current and an airstream were measured at a non-zero value. The airflow is measured with a Testo 405i hot wire anemometer (Testo SE & Co. KgaA, Celsiusstrasse 2, 79822 Titisee-Neustadt. Accuracy +/- 0.1 m/s, Resolution 0.01 m/s, Measuring time interval 2 s.) From there on, each measurement point was run for several minutes in order to establish stationary conditions. In particular, with dielectric studies, stationary conditions were necessary as charges tend to accumulate on the enclosing walls, thus reducing the electric current.

In near-breakdown voltage experimental runs, the variation of airspeed over time is large; hence a minimum, maximum and time-averaged value for the airspeed is reported.

Table 1: Measurements overview.

Config.	Regulated variables					Measured variables					
	Voltage	Electrode Distance	Nozzle gap	Dielectric height	Mesh	Electric Current	Temper-ature	Humidity	Airspeed		
									M1	M2	M3
	ϕ [kV]	δ [mm]	h [mm]	ε [mm]	[mm]x[mm]	I [μA]	T [°C]	φ [%]	w [m/s]		
(a)	0-32	50	n/a	n/a	150 x 150					✓	
(b)	0-32	25 / 50	n/a	n/a	150 x 10					✓	
(c)	0-32	25	n/a	15/35/85	150 x 10	✓	✓	✓		✓	
(d)	0-32	25	10/20	85	150 x 10					✓	
(e)	0-32	25	10	35	150 x 10				✓	✓	✓

3.3 Performance evaluation metrics

The operation range of the EHD air amplifier is primarily defined by its voltage-current characteristics. These characteristics show how much electric current is flowing at a specific voltage. By definition, the EHD air amplifier operation range starts when both an electric current and an airstream are measured. Note that a Corona discharge may be measurable well before EHD air amplification occurs.

With the current-voltage ($I-U$) characteristics, the power consumption P is straightforwardly determined from

$$P = UI \tag{1}$$

Another measured value is velocity. At different locations, the value is taken from point probes anemometers. For the amplification mechanisms, we are interested in the volumetric flow rates [m^3/s], which are estimated as

$$\dot{V} = \overline{w} A_{cs} \tag{2}$$

where $\overline{w}$ [m/s] is the time-averaged speed at the measurement point and A_{cs} [m^2] is the cross-sectional area of the measurement point location. With the volumetric flow, we also estimate the amplification factor AF from

$$AF = \frac{\dot{V}_{out}}{\dot{V}_{in}} \tag{3}$$

The amplification factor is esimated here based on the air velocity measured at one point in the channel, for this proof of concept study. For future optimization of the EHD air amplifier, it would be beneficial to measure the air velocity profile via multiple point measurements or via laser diagnostics (e.g., particle image velocimetry). Furthermore, we assess the performance of EHD air amplification benchmarked to regular EHD and other airflow propulsion devices by the performance number γ which has the units (m^3/h)/W:

$$\gamma = \frac{\dot{V}_{out}}{P} \tag{4}$$

3.4 Statistical data evaluation

Three replications of the measurements are done and the results are expressed as average ± standard deviation for electrical parameters. For flow-related measurements, the data is measured over a 1-minute period. The results of flow speed are reported as min/max range. The results for flow rate are derived from the average of the velocity measurements. To obtain flow rate and flow rate to power characteristics, the results for flow rate are assisted by Local Polynomial Regression Fitting (LOESS) for display with a 0.95 confidence interval ribbon. The statistical analysis has been performed in R [13].

4 Results

4.1 EHD free field power demand for wire and needle

Figure 4 compares the electric power demand of both needle and wire for the EHD free field case, i.e., the base configuration with the large mesh at 50 mm spacing. The most apparent difference between needle and wire in power consumption is the EHD onset voltage. The needle can produce a measurable current and airflow at 9 kV. With the wire, the onsets at 15 kV. Both are similar in terms of power consumption, especially at higher voltages. Note that the EHD onset voltage is different from Corona discharge onset voltage. The EHD onset voltage requires both an airstream and an electric current to be non-zero. At lower voltages, the Corona onset starts at 15 kV for the wire and the power demand is about 70 % lower than for needles. With a rather large inter-electrode gap of 50 mm even a finer mesh would produce similar results. For engineering purposes, one would want to create a discharge at the lowest possible voltage to leave more room for finetuning the airflow.

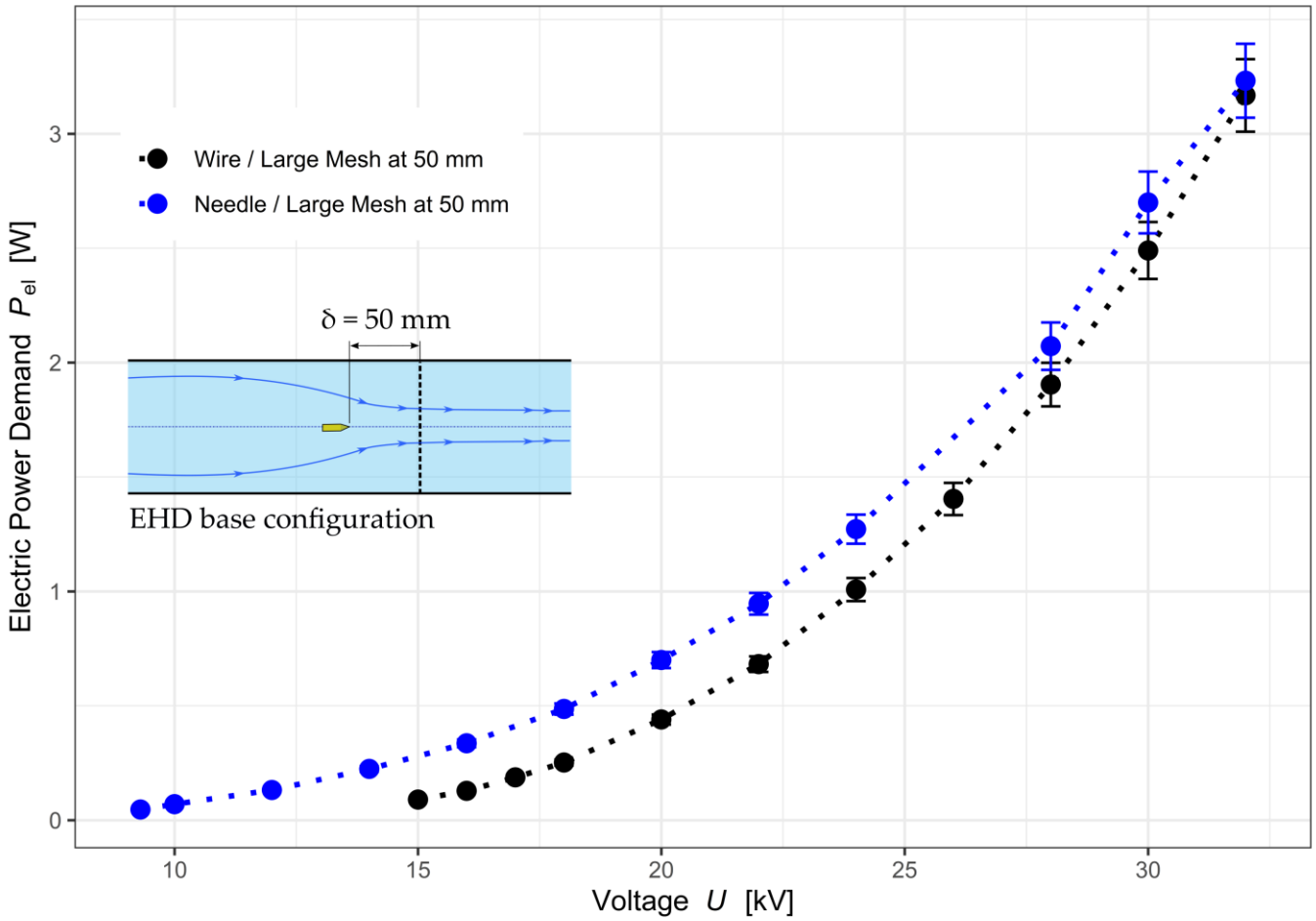

Figure 4: Power demand curves for the base configuration, i.e., free flow EHD. The wire consumes less power, but the EHD onset happens only after 15 kV, which means a decreased operational range.

4.2 Impact of reducing the collector electrode size on power demand

Figure 5 compares the results of configuration (b), where the influence of the electrode configuration is studied. Direct comparison between needle and wire emitter electrodes shows that needles consume more power, i.e., produce a more intense electric current.

Similar behavior was also observed in the free field EHD configuration. As far as the Corona onset voltage is concerned, the large mesh at 50 mm distance behaves similarly to a small mesh at 25 mm distance for both needles and wires. However, with increasing voltage, the differences in power consumption become more pronounced, i.e., small meshes at closer distances demand considerably more current. The wire / small mesh at 25 mm case reaches the spark-over voltage already at 22 kV while its onset is at 15 kV. This case has the narrowest operation range and poses a handicap for successful EHD air amplification.

Another direct comparison between needle and wire cases for both small and large mesh at the same distance (50 mm) shows that the smaller mesh tends to reduce power demand, which is in agreement with general expectations as the number of conducting ground surfaces is reduced [2]. Here we can also observe that the power demand reduction from large to small mesh ground is considerably more significant for wire emitters than for needles. Needles react less sensitive to the size as they can transmit more power even in downsized electrode configurations. This observation is vital in the design of future downsized configurations. In summary, we can reduce successfully the size of the collector and should prefer, at this point, to use a needle emitter. For downsizing purposes, the needle performs best as it yields the overall most extensive operation range.

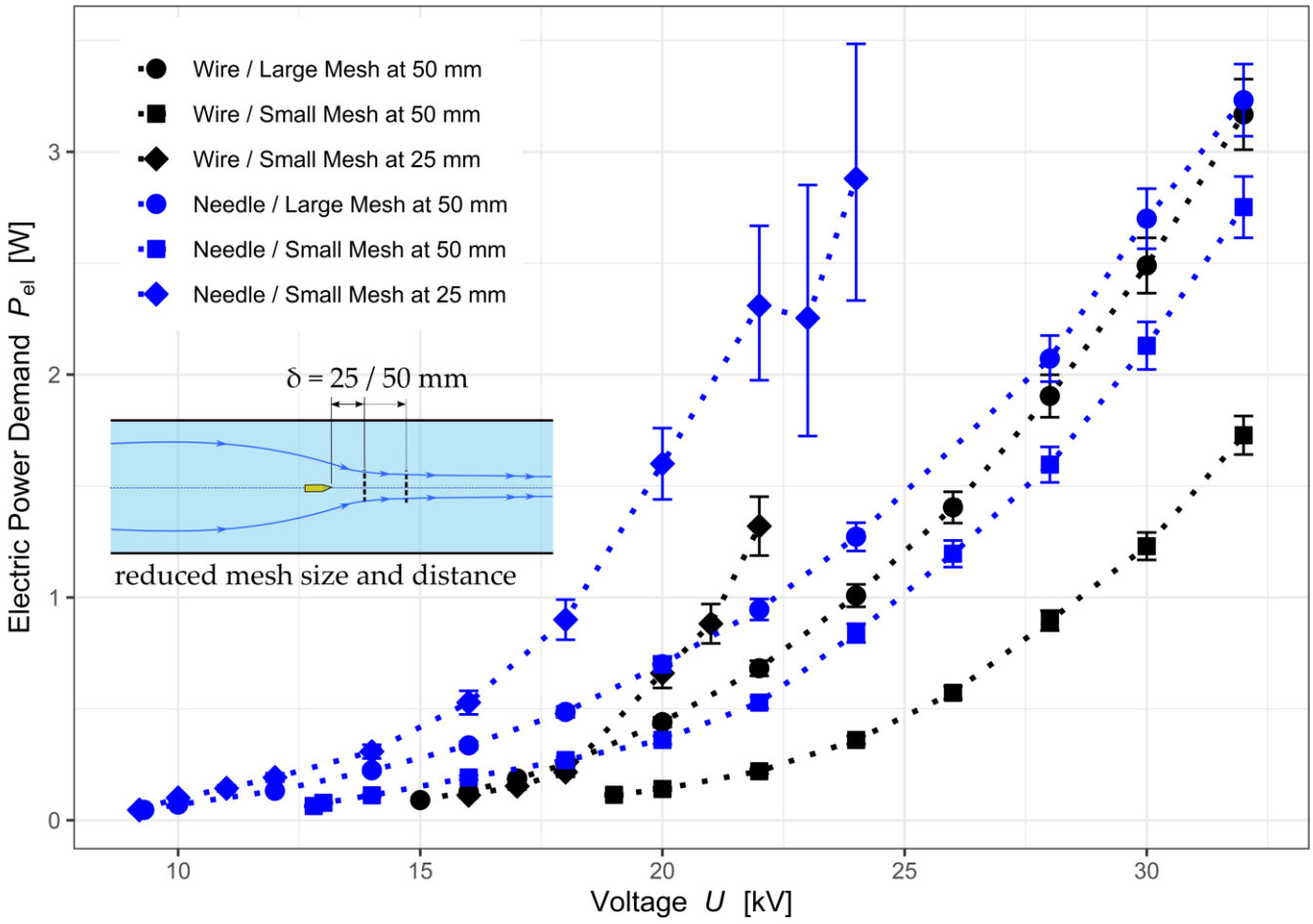

Figure 5: Power demand curves for configuration (b) with reduced mesh collector and distance. A larger voltage operation range for needles can be observed, especially at larger distances. At short distances, needles trigger EHD airflow below 10 kV, whereas the wire starts producing airflow at 15 kV. However, with short distance the Corona discharge tends to become unstable (as per error bars) at voltages above 21 kV. This phenomenon is more pronounced with the needle and small mesh at 25 mm. The unstability at higher voltages emerges as a consequence of intensity variations in the electric field. The mesh collector itself consists of sufficiently thin wires that are increasingly distorting the potential distribution at such elevated voltages.

4.3 Impact of dielectric material on discharge stability and operation range

The presence of a nearby dielectric, i.e., two acrylic glass plates as in case (C) in Figure 3, leads to a distortion of the electric field due to the different relative electric permeability ($\varepsilon_r \approx 1$, for air and $\varepsilon_r \approx 5$, for acrylic glass). This distortion decreases the inhomogeneity of the electric field on the emitter electrode, which is essential to maintain a sustained Corona discharge [14]. As such, the breakdown stability and operation range are strongly affected by the presence of a nearby dielectric.

The operation range is shown in Figure 6 through the current-voltage characteristics for the small mesh case. The most apparent difference between needle and wire is the shift in Corona onset voltage which starts at 9 kV for needles and 17 kV for the wire electrodes. Moreover, the discharge on the wire seems to suffer from the presence of the dielectric. The current magnitude decreases rapidly. This is an indicator that the electric field is distorted unfavorably for the wire setup. In principle, the electric field lines

bend under influence of the dielectric such that the propagation of ions becomes more symmetric around the emitter. This causes the ions to accelerate towards the side walls which weakens the discharge stability due to local accumulation of charges.

On the other hand, needles are less affected by the presence of acrylic glass plates. The electric current reduces with an approaching dielectric, but it remains active nonetheless. Also, the spark over voltage is at 24-26 kV, which leaves a spectrum of about 15 kV for the operation range (about three times larger than for wires).

It is desirable to maintain an extensive operation range in terms of voltage and continuous production of ions. This is given for needles as they retain the best discharge stability. Hence, only needles are considered for the final EHD air amplification configuration, despite the fact that wires seemed at first to provide lower electric power demand when sizing down the electrodes.

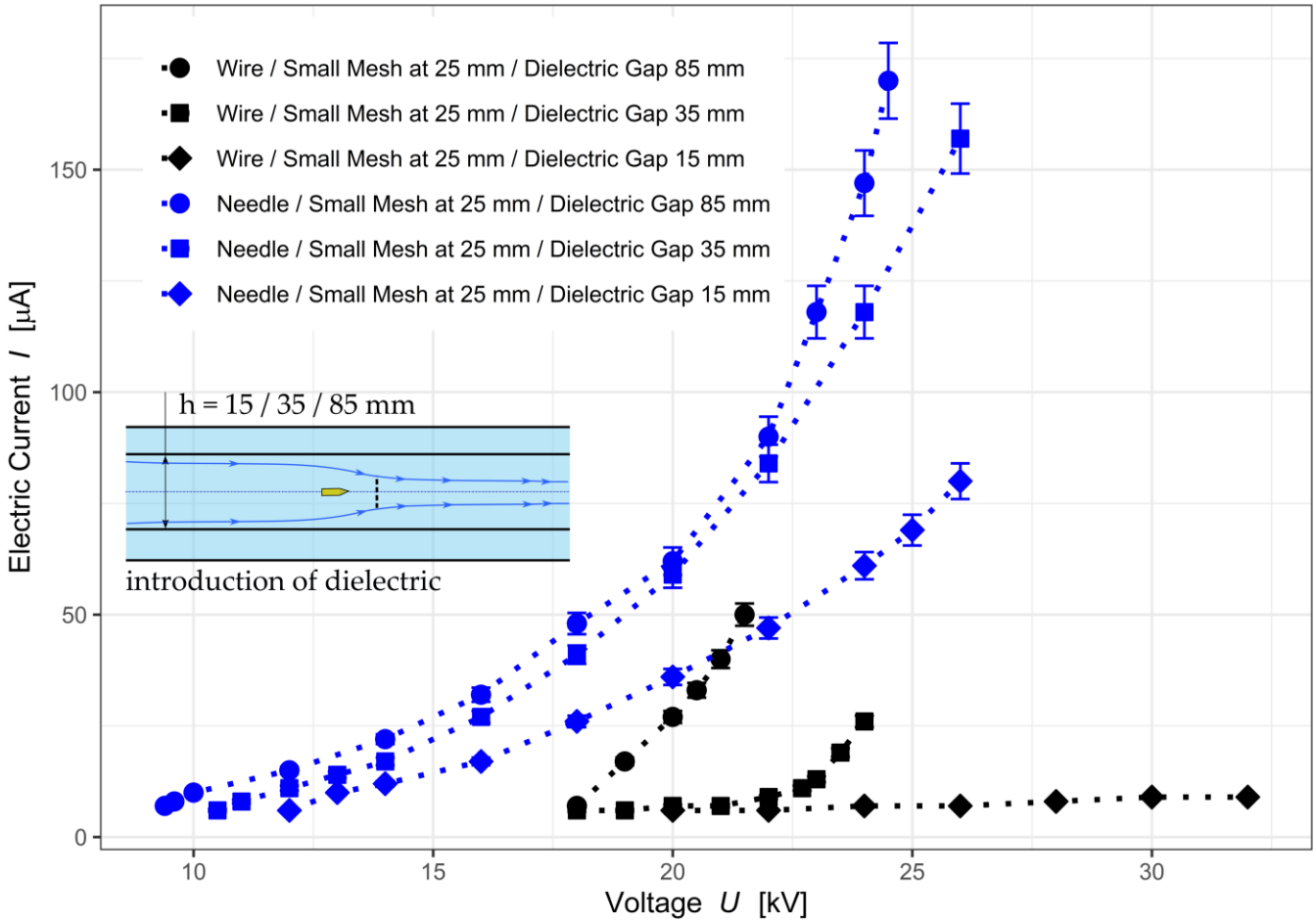

Figure 6: Voltage-current characteristics for configuration (C), including two acrylic glass plates at a variable gap distance. We note here that the dielectric has both a stabilitzing and attenuation effect on the discharge. The attenuation is more pronounced on the wire electrode. The operation range is strongly reduced and for the smallest dielectric gap the discharge is impeded. The needle electrodes, on the other hand, profit from the dielectric-dependent distortions in the electric field by emitting less charge and in a more stable way over the entire operation range.

4.4 Impact of airflow contraction on the outlet velocity fluctuations

We require to accelerate the airflow to successfully create a Coanda effect and entrain airflow in the air amplifier. The converging nozzle increases the outflow speed by contraction and it also poses a flow resistance and decreases static pressure.

In Figure 7, the center speed at the outlet is reported for the 85 mm dielectric gap case with the nozzle at different sizes and without the nozzle. The measured velocity is a spread between the maximum and minimum observed velocity. The fields for needle and wire barely overlap. Both wire and needle have in common that the variation is large without a nozzle. Here, the needle emitter also proves more useful to generate faster speeds, which ultimately benefits the propulsion of air on a flat plate to produce EHD air amplification.

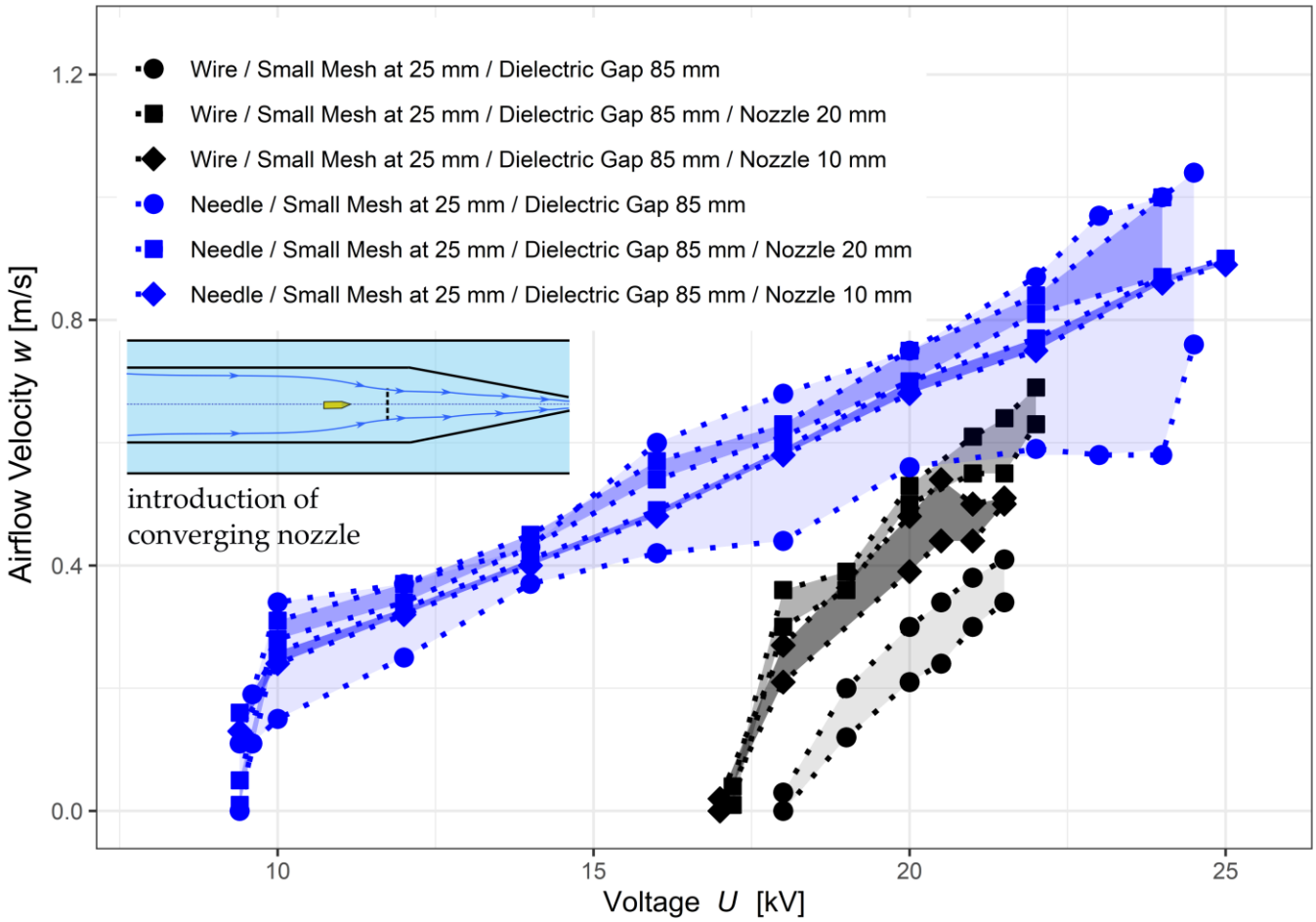

Figure 7: Airflow velocity at the outlet center of the channel. Without a nozzle, the air velocity varies over a more extensive range. A nozzle helps in reducing the air velocity variations.

4.5 Proof of concept of EHD air amplification

In this section we will show that the Coanda effect triggers air amplification with EHD. Figure 8a reports the time-averaged air flow rates at measurement locations according to the sketch in Figure 3e. M3 is the point probe that tracks the amplified flow rates, i.e., airflow generated as a result of the Coanda effect. M1 tracks the velocity within the EHD channel alone, while M2 is the total flow rate. The shaded areas represent the 0.95 confidence interval. It can be observed that for the EHD channel, the fluctuations are small in time, i.e., a constant inflow can be obtained.

The corona discharge onset voltage to measure the minimum airstream is at 10 kV. Until 12 kV, the airflow at the inlet is dominant, and shortly after, M2 experiences a jump in flow rates. This is the point where EHD air amplification starts to develop. At 16 kV, an airflow can also be measured at M3, thus proving the proof-of-concept that EHD air amplification is feasible. With the current setup, amplification factors of up to almost 3 are achieved as seen in Figure 8b.

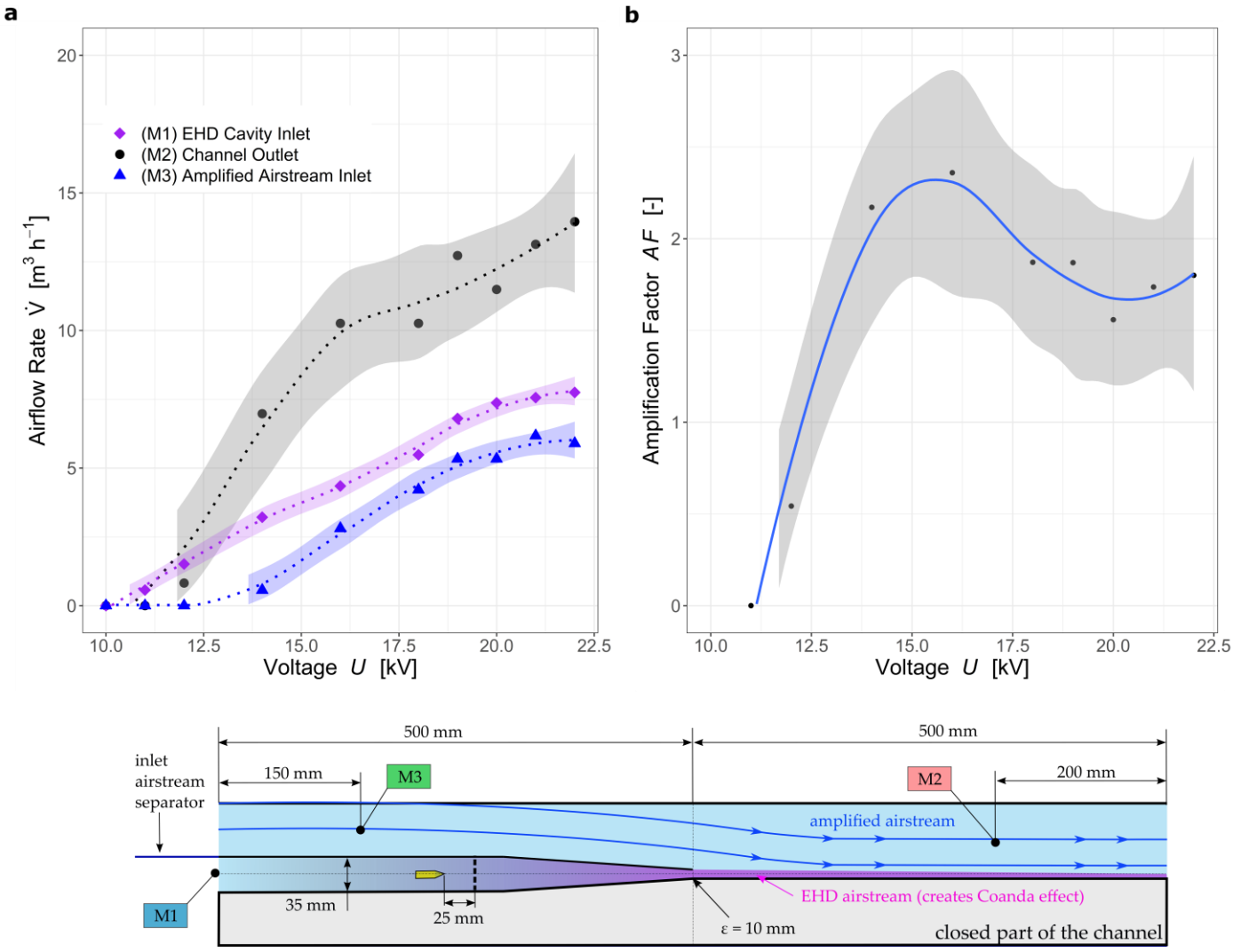

Figure 8: (a) Time-averaged airflow rates at three different EHD air amplifier configuration locations and (b) the resulting amplification factor.

To benchmark EHD air amplification to regular EHD, the amplified airstream inlet is blocked, and the measurements are repeated. At location M3, for the benchmark case, zero airflow is measured. At outlet M2, the flow rate is taken and compared to previously determined data. Figure 10 shows that EHDAA yields an up to 75% efficiency gain compared to the regular EHD benchmark case. Also, we observe that with increasing voltage, the increasing current does not provide more substantial flow. Instead, that stream seems to dissipate electrical power without bringing additional momentum transfer. The reason herefore is that EHD-generated flow scales with sufficient precision linearly with voltage while the power consumption exhibits a strong non-linearity with increasing voltage. Air amplification increases the flow rate after the Coanda effect establishes and thus shifts the flow per power ratio significantly. Hence, an efficiency maximum is achieved shortly after the Corona onset voltage. In summary, we can produce EHD air amplification with amplification factors up to three. This is lower than current air amplifiers but it is a start for further optimization.

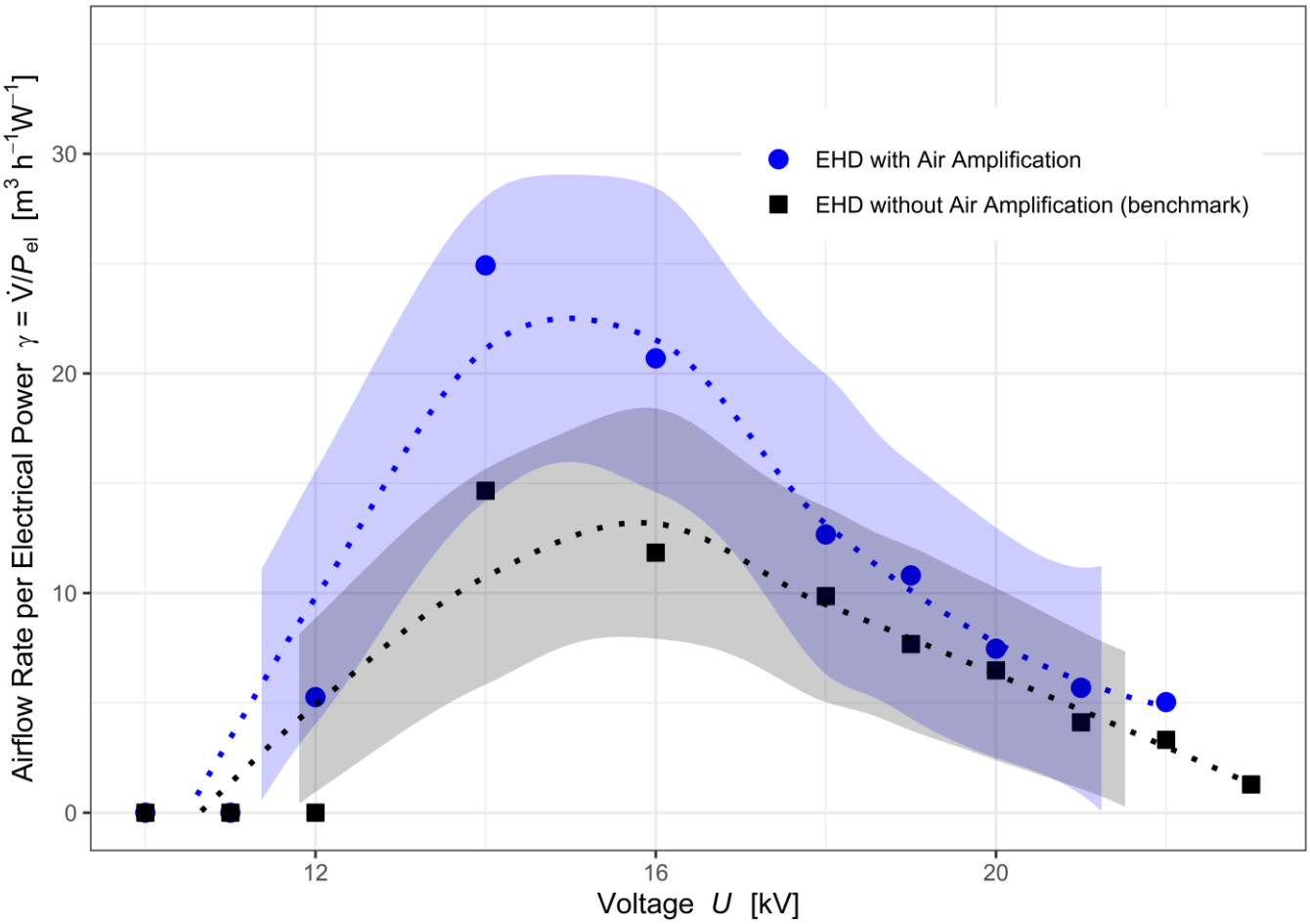

Figure 9: EHD air amplification benchmark against regular EHD without air amplification. The air amplification configuration yields up to a 66 % efficiency increase.

5 Discussion

We analyzed in a step-wise manner the feasibility of EHD air amplification. To achieve EHD air amplification in this study, we used five rig configurations, two emitting electrode types, and two mesh electrode sizes. The arrangement and type of electrodes themselves offer vast optimization potential. We thus only explored a small set of the parametric space. This was however sufficient for the aim of the study, namely to show the proof of concept.

In our study, the needle outperformed the wire as it allowed for a more extensive operation range due to its increased discharge stability. The reason for this superior stability is that needles have a more inhomogeneous electric field at the tip. We could show that a nearby dielectric may impede the discharge. However, the needle maintains its inhomogeneity nonetheless. Therefore, we conclude that the needle is the most suitable emitter type for EHD air amplification. In free-flow EHD, the wire may be more efficient in generating flow rates. However, in EHD air amplification, we need to put the electrodes within a non-conducting enclosure which introduces homogeneities in the electric field. However, our study is limited to the proposed needle shape, and other shapes, tip curvatures, and distances may be more suitable. A comprehensive study featuring the needle geometry will be carried out in the future.

On the airflow side, we showed a concept that achieves amplification factors up to 3. Other settings and arrangements such as number of needles or nozzle shapes could potentially benefit from exploiting the Coanda effect. EHD air amplification operates at low pressures compared to conventional, pressurized-air amplifiers. However, this new way of combining EHD and the Coanda effect at low pressure also benefits energy-wise. For example, the peak energy efficiency is reached somewhere after the onset of Corona discharge and maintains a relative energy efficiency that is higher even with increasing flow rates.

To compare the benefits of EHD air amplification to state-of-art technologies, **Error! Reference source not found.** gives an overview of the operation range of industrial and consumer air amplifiers and an axial fan (Type 5318 /2 TDHHP, 66 W, 490 m³/h, ebm-papst St. Georgen GmbH, Hermann-Papst-Str. 1, D-78112 St. Georgen). The power demand P_d [W] of the Meech product is calculated assuming compression of air as an ideal gas

$$\left| P_d = p_{sup} \dot{V}_{sup} \ln\left(\frac{p_0}{p_{sup}}\right) \right| \quad (7)$$

which estimates the power needed to raise the supplied airflow $\dot{V}_{sup}$ [m^3h^{-1}] the pressure from ambient pressure $p_0 = 1$ atm to supply pressure p_{sup}. **Error! Reference source not found.** also lists the electrohydrodynamic (EHD) air amplifier investigated in this study. It becomes apparent that air amplifiers fed by pressurized per se are not very energy efficient. This is because supplying pressurized air costs lots of energy. The size of an air amplifier significantly impacts its capability to deliver flow rate per power, e.g., larger dimensions favor efficiency in terms of flow rate to power ratio. The large Dyson Purifier Cool performs best in delivering flow rates per electric power invested. But that is mainly due to its size. When taking into account the surface area of the device we obtain the average speed to power ratio. This metric makes comparison possible across all devices. Here, the the Dyson Purifier Cool does not perform significantly better than a pressurized-air fed air amplifier. It also underperforms compared to an axial fan. The EHD air amplifier shown as a result of this study produces flow rates at a significantly lower energy cost.

Table 2: Air amplification devices overview and axial fan for comparison

Device	Size	Amplification Factor (AF)	Output flow rate	Average air speed	Supply pressure	Power demand	Flow rate to power ratio	Average speed to power ratio
Unit	[mm]	[-]	[$m^3\,h^{-1}$]	[m/s]	[bar]	[W]	[$m^3\,h^{-1}W^{-1}$]	[$m\,s^{-1}W^{-1}$]
Meech Air Amplifier	100 (diameter)	25	638	22.6	1.4	321	1.99	0.07
Dyson Supersonic	32.4 (diameter)	Unknown	46.8	15.8	Unknown	1600	0.03	0.01
Dyson Purifier Cool	638 x 135 (rectangular)	Unknown	1044	3.4	Unknown	40	26.1	0.09
Axial Fan	134 (diameter)	n/a	490	9.7	n/a	66	7.42	0.15
EHD Air Amplifier	150 x 80 (rectangular)	3	7.5	0.23	ambient	0.3	25	0.76

For further comparison, EHD can also deliver a certain supply pressure, but this supply pressure is considerably lower than what we see for commercially established devices. An estimation of EHD pressure is possible via the following expression [12]

$$p = \frac{I \cdot d}{b \cdot A_G}. \quad (8)$$

with I being the electric current [A], d the distance [m] between the emitter and collector, b the ion mobility ($b = 2 \cdot 10^{-4}\ m^2/(V \cdot s)$) and A_G the cross-section [m^2] of the corona discharge. The cross-section may be taken at any point within the conical shape of the space charge area along with its corresponding current and distance. Some typical values for EHD-driven blowers are a cross-section of $A_G = 1200\ mm^2$ at a current of $I = 100$ µA and a distance of $d = 50$ mm. This gives an EHD supply pressure of approximately 5 Pa. This is considerably lower than the devices we have evaluated so far.

By combining EHD with low-pressure air amplification technology, we aim to create a concept that increases the currently low energy conversion efficiency of EHD-driven devices. EHD air amplification outperforms even an axial fan in this example. Moreover, EHD air amplification retains the benefits of corona discharge, e.g., ozone production, which can interest decontamination applications.

6 Conclusions

Electrohydrodynamic (EHD) air amplification was investigated experimentally. Our goal was to increase EHD-generated airflow rates to improve the low conversion rate of electrical energy from ionic wind to mechanical energy. To this point, EHD airflow generation improvements have focused on electrode arrangements. This study is the first to combine EHD with air amplification to ramp up flow rates and thus increase the overall performance. In contrast to conventional air amplifiers fed by pressurized air, EHD air amplification operates at near atmospheric pressure. With the view to further improve EHD air amplification, the key findings of this study are:

- Needle electrodes outperform wire electrodes in terms of discharge stability. The EHD operation range for wires is 16 to 24 kV and for needles 9 to 25 kV (+100 %).
- Dielectrics in proximity of the discharge electrodes drastically reduce the power demand by lowering the current flow. Wire electrodes may even cease operation as their discharge onset is shifted towards higher voltages (17 kV) while needle electrodes keep producing current from 9 kV on (-52 %).
- The peak energy performance in flow rate per electrical power invested substantially increases from 15 to 25 (m^3/h)/W (+66 %) compared to a non-amplifying EHD benchmark.

- By exploiting the Coanda effect where the EHD-generated airstream is directed towards a plate, another airstream is induced, up to three times higher. Thus, leading to an amplification factor of up to 3.

This experimental study demonstrates the feasibility and potential to generate higher EHD-based flow rates at low pressures with little energy input. Upcoming studies focus on the optimization of EHD air amplifiers to further increase flow rates and amplification factors while also reducing energy consumption. Much can be achieved by finetuning the geometrical arrangement of electrodes which ultimately opens the doors for downsized EHD air amplifiers. In this regard, we will also consider EHD air amplifiers for external flows, which will further improve our solution by exploiting the Coanda effect. Numerical simulations ideally assist these optimization studies.

Acknowledgments

The authors are grateful to the Swiss Innovation Agency (Innosuisse 34549.1 IP-LS) for the financial support provided during project conceptualization and execution.

AUTHOR CONTRIBUTIONS

Donato Rubinetti: Conceptuatlization, Methodology, Investiation, Project Management, Writing – review and editing. Kamran Iranshahi: Methodology, Writing – review and editing. Daniel Onwude: Writing – review and editing. Lei Xie: Methodology, Writing – review and editing. Bart M. Nicolaï: Writing – review and editing. Thijs Defraeye: Conceptualization, Methodology, Supervision, Funding procurement, Project Management, Writing – review and editing.

REFERENCES

[1] T. Defraeye and A. Martynenko, "Electrohydrodynamic drying of food: New insights from conjugate modeling," *J. Clean. Prod.*, vol. 198, pp. 269–284, Oct. 2018, doi: 10.1016/j.jclepro.2018.06.250.

[2] K. Iranshahi, A. Martynenko, and T. Defraeye, "Cutting-down the energy consumption of electrohydrodynamic drying by optimizing mesh collector electrode," *Energy*, vol. 208, p. 118168, Oct. 2020, doi: 10.1016/j.energy.2020.118168.

[3] D. F. Colas, A. Ferret, D. Z. Pai, D. A. Lacoste, and C. O. Laux, "Ionic wind generation by a wire-cylinder-plate corona discharge in air at atmospheric pressure," in *Journal of Applied Physics*, Nov. 2010, vol. 108, no. 10, p. 103306, doi: 10.1063/1.3514131.

[4] R. Tirumala and D. B. Go, "Multi-electrode assisted corona discharge for electrohydrodynamic flow generation in narrow channels," *IEEE Trans. Dielectr. Electr. Insul.*, vol. 18, no. 6, pp. 1854–1863, Dec. 2011, doi: 10.1109/TDEI.2011.6118623.

[5] N. E. Jewell-Larsen, E. Tran, I. A. Krichtafovitch, and A. V. Mamishev, "Design and optimization of electrostatic fluid accelerators," *IEEE Trans. Dielectr. Electr. Insul.*, vol. 13, no. 1, pp. 191–203, Feb. 2006, doi: 10.1109/TDEI.2006.1593417.

[6] S. Kanazawa, W. Imagawa, S. Matsunari, S. Akamine, R. Ichiki, and K. Kanazawa, "Ionic Wind Devices Prepared by a 3D Printer." Accessed: Oct. 14, 2021. [Online]. Available: https://ijpest.securesite.jp/Contents/11/1/PDF/11-01-038.pdf.

[7] M. Rickard, D. Dunn-Rankin, F. Weinberg, and F. Carleton, "Maximizing ion-driven gas flows," *J. Electrostat.*, vol. 64, no. 6, pp. 368–376, Jun. 2006, doi: 10.1016/j.elstat.2005.09.005.

[8] T. Panitz and D. T. Wasan, "Flow attachment to solid surfaces: The Coanda effect," *AIChE J.*, vol. 18, no. 1, pp. 51–57, Jan. 1972, doi: 10.1002/aic.690180111.

[9] A. Dumitrache, F. Frunzulica, and T. C. Ionescu, "Mathematical Modelling and Numerical Investigations on the Coanda Effect," in *Nonlinearity, Bifurcation and Chaos - Theory and Applications*, InTech, 2012.

[10] M. Robinson, "Movement of air in the electric wind of the corona discharge," *Trans. Am. Inst. Electr. Eng. Part I Commun. Electron.*, vol. 80, no. 2, pp. 143–150, 2013, doi: 10.1109/tce.1961.6373091.

[11] D. Rubinetti, K. Iranshashi, D. Onwude, L. Xie, B. Nicolai, and T. Defraeye, "An in-silico proof-of-concept of electrohydrodynamic air amplifier for low-energy airflow generation," doi: 10.31224/2436.

[12] E. Moreau, N. Benard, J. D. Lan-Sun-Luk, and J. P. Chabriat, "Electrohydrodynamic force produced by a wire-to-cylinder dc corona discharge in air at atmospheric pressure," *J. Phys. D. Appl. Phys.*, vol. 46, no. 47, p. 475204, Nov. 2013, doi: 10.1088/0022-3727/46/47/475204.

[13] "RStudio | Open source & professional software for data science teams - RStudio." https://www.rstudio.com/ (accessed Mar. 03, 2022).

[14] M. J. Johnson, R. Tirumala, and D. B. Go, "Analysis of geometric scaling of miniature, multi-electrode assisted corona discharges for ionic wind generation," *J. Electrostat.*, vol. 74, pp. 8–14, Apr. 2015, doi: 10.1016/J.ELSTAT.2014.12.001.